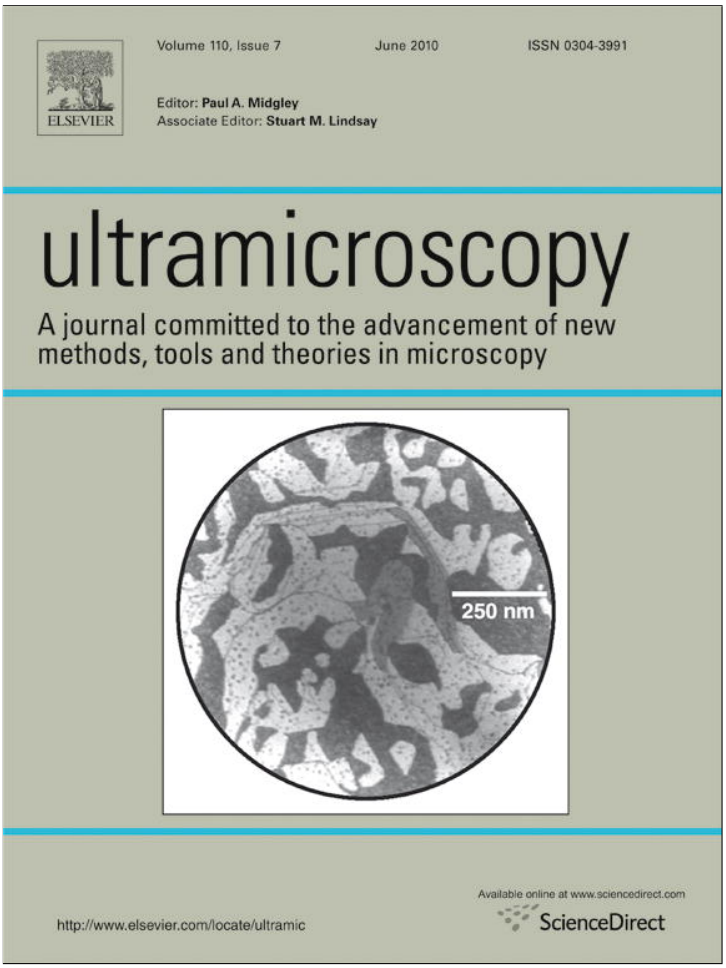

Ultramicroscopy 110 (2010) 820–825

Contents lists available at ScienceDirect

Ultramicroscopy

journal homepage: www.elsevier.com/locate/ultramic

Identification of magnetic properties of few nm sized FePt crystalline particles by characterizing the intrinsic atom order using aberration corrected S/TEM

Johannes Biskupek [a,*], Joerg R. Jinschek [b], Ulf Wiedwald [c], Markus Bendele [c,1], Luyang Han [c], Paul Ziemann [c], Ute Kaiser [a]

[a] Central Facility of Electron Microscopy, Ulm University, Albert-Einstein-Allee 11, D-89081 Ulm, Germany
[b] FEI Nanoport Europe, NL-5600 Eindhoven, Netherlands
[c] Institute of Solid State Physics, Ulm University, D-89081 Ulm, Germany

ARTICLE INFO

Article history:
Received 24 October 2009
Received in revised form
16 February 2010
Accepted 21 February 2010

Keywords:
Aberration corrected HRTEM
Aberration corrected STEM
FePt
Image calculation
Chemical order
Magnetic nanoparticle

ABSTRACT

Hard-magnetic nanomaterials like nanoparticles of FePt are of great interest because of their promising potential for data storage applications. The magnetic properties of FePt structures strongly differ whether the crystal phases are face centered cubic (fcc) or face centered tetragonal (fct). We evaluated aberration corrected HRTEM, electron diffraction and aberration corrected HAADF-STEM as methods to measure the chemical degree of order S that describes the ordering of Pt and Fe atoms within the crystals unit cells. S/TEM experiments are accompanied by image calculations. The findings are compared with results obtained from X-ray diffraction on a FePt film. Our results show that STEM is a reasonable fast approach over HRTEM and electron diffraction to locally determine the chemical degree of order S.

1. Introduction

Hard-magnetic nanoparticles are of great interest because of their promising potential for data storage applications [1], sensor devices [2] or medical treatments [3]. Current synthesis techniques like the micellar approach [4] or gas-phase preparation [5] allow precise production of magnetic nanoparticles from 2 to 15 nm consisting of FePt or CoPt with a narrow size distribution at equiatomic composition [4]. The magnetic properties of such tiny compound magnets are directly related to the structural (dis)ordering of Fe, respectively, Co, and Pt atoms on the atomic scale. For understanding this particular structure–property relationship, a structural analysis method with high spatial resolution and high chemical sensitivity is essential.

$Fe_{50}Pt_{50}$ alloys are mostly prepared in the disordered face centered cubic (fcc) crystal structure [6] with Fe and Pt atoms randomly distributed within the crystals unit cell. In the composition window of roughly 40–65% Fe atom fraction [7], a transition into the face centered tetragonal (fct) phase (also called $L1_0$ phase) occurs at elevated temperature of 450 °C in thin films and of 650 °C in nanoparticles, respectively [6]. This transition is accompanied by structural ordering of Fe and Pt atoms in bi-layers along [0 0 1] direction: one layer only consists of Fe atoms, the other only of Pt atoms. This ordering goes along with a small compression of the c-axis of the unit cell, i.e. the lattice parameter ratio c/a changes. Any intermediate degree of chemical order can be described by the order parameter $S=2P-1$, where P is the fraction of Fe (Pt) atoms on their specific sites in the unit cell. S ranges from 0% (pure fcc phase) to 100% (perfect fct phase). This structural property, described by S, is directly linked to the magnetic properties of FePt (in case of Fe:Pt=50:50) for bulk systems [8]. The perfectly ordered fct phase has a magnetocrystalline anisotropy energy density (MAE) of 6×10^6 J m^{-3} that is up to 60 times larger than that of the disordered fcc phase with 1×10^5 J m^{-3} [9].

The parameter S can be easily determined on films of FePt using X-ray diffraction either comparing the intensities of (0 0 2) reflection (valid for fcc and fct phase) and (0 0 1) reflection (valid only for fct phase) or by determining the ratio of a- and c-lattice parameters e.g. [10,11]. However, for small FePt particles deposited on a crystalline support such as (1 0 0) MgO, X-ray

* Corresponding author.
E-mail address: Johannes.Biskupek@uni-ulm.de (J. Biskupek).
[1] New address: Institute of Physics, Zürich University, CH-8057 Zürich, Switzerland.

0304-3991/$ - see front matter © 2010 Elsevier B.V. All rights reserved.
doi:10.1016/j.ultramic.2010.02.043

diffraction cannot be applied for two reasons: (i) it does not give sufficient signal from the FePt nanoparticles and (ii) the c/a ratio cannot be used as the FePt grows epitaxial on MgO(001) with large strain (MgO and FePt have a lattice misfit of about 10%).

Magnetic properties of those structures are usually measured using superconducting interference devices (SQUID) or the X-ray magnetic circular dichroism (XMCD) integrating over a large number of particles e.g. [4,8]. However, properties of single particles cannot be accessed by those methods. Microscopic techniques, such as Lorentz microscopy and electron holography, allow determining magnetic properties of single nanoparticles [12,13]. However, spatial resolution is currently limited to a few nanometers. The sensitivity of the method in terms of magnetic detection limit depends on the precision to detect small shifts of the phase of the electron wave that is currently about $\pi/30$. This is not sufficient to measure the magnetic properties of FePt particles with sizes smaller than 5 nm.

Structural and chemical information on the atomic scale (i.e. Ångstrøm and or even sub-Ångstrøm resolution) could be accessed by the latest generation scanning/transmission electron microscopes (S/TEM) equipped with aberration correctors [14–16]. Free standing fcc and fct FePt particles have already been studied by Dmitrieva and co-workers [17–19] using quantitative HRTEM accompanied by image calculations. In these previous works the ratio of FePt particles that are showing features of the fct phase versus particles that are showing features of the fcc phase was determined in dependence of the preparation or treatment of the particles. Particles that are in an intermediate state e.g. the chemical degree of order is $S=0.5$ have been categorized either on the side of pure fct particles or of pure fcc particles. FePt particles [20] and FePd particles [20–22] were studied by Sato and co-workers by aberration corrected TEM and nanobeam diffraction. In these works ordering effects of the particles were investigated showing a size-dependent ordering as well lattice parameter changes because of composition changes.

In our present work, we are going to explore the possibilities of corrected S/TEMs to determine the atomic structure and the parameter S of FePt films and particles by S/TEM experiments combined with image calculation. Because the chemical degree of order S and magnetic properties are directly linked to each other for bulk systems and strain-free thin films, our local structural analysis utilizing S/TEM could supersede or even replace integrating methods such as XMCD or SQUID. In our special case, aberration corrected S/TEM can moreover fill the lower gap in magnetic information retrieval that cannot be covered yet because of either resolution or sensitivity limitations in Lorentz microscopy and in Lorentz electron holography.

Here, we are evaluating on the basis of image and diffraction calculations the appropriate corrected S/TEM method to determine the order degree S in FePt nanoparticles and thin films. The appropriate S/TEM experiments on a FePt film are compared with the results obtained from X-ray diffraction of the identical FePt film prior TEM sample preparation.

2. Materials and methods

FePt particles (average diameter 5 nm) with epitactic relationship to MgO substrate have been prepared using dip-coating of Fe- and Pt-salt loaded micelles on MgO followed by subsequent oxygen and hydrogen plasma etching and thermal annealing (see [4] for details). A thin film (10 nm) of SiO_2 was deposited on top of the particles to protect the particles from oxidation prior to TEM sample preparation.

Thin films of FePt (30 nm) on MgO have been prepared using pulsed laser deposition (PLD) followed by annealing (see [23] for details). The parameter S has been determined by X-ray diffraction measuring the ratio of (0 0 1) and (0 0 2) reflections.

TEM samples have been prepared using standard cross-section techniques i.e. cutting of stripes and gluing them, mechanical grinding and polishing followed by low angle Ar-ion milling. TEM investigations were carried out using aberration corrected imaging and scanning systems of the type FEI Titan 80–300 microscope operating at 300 kV. The aberrations were tuned until a phase plate of better than 20 mrad was reached in accordance to the $\pi/4$ criteria. The residual errors of the measurements of the aberrations (printout of CEOS' corrector software) were larger than the measured aberrations (e.g. coma B_2 better than 20 nm, spherical aberration, 4-fold astigmatism A_3 better than 1 μm). The spherical aberration C_S was chosen to be slightly negative at (-5 ± 1) μm to optimize the contrast for the case of HRTEM imaging [24]. Aberration corrected high resolution (HR) TEM images have been acquired using a Gatan Ultrascan 1000 slow scan CCD camera. Corrected Z-contrast STEM images were acquired using a Fischione HAADF detector. The collection angles for HAADF detector were between 40 and 200 mrad (small camera length). STEM images were digitally processed for better visualization using a Wien-filtering technique to lower the scanning noise artefacts without losing the information of the intensities. Using the FFT of the images, masks with 10 pixel radii including a 3 pixel wide cuff-off were positioned around the 0 0 0 reflections (intensity information) and the Bragg-reflections (atomic column position information). After applying the mask,

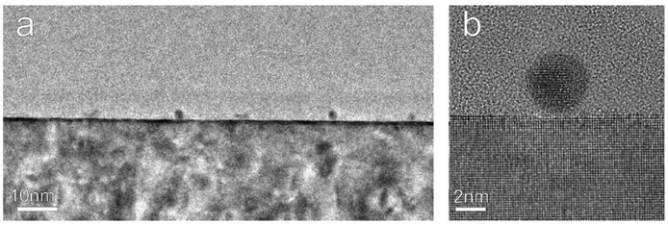

Fig. 1. FePt nanoparticles on (1 0 0) MgO. (a) Overview of the bright-field TEM image showing regular particles on top of MgO and (b) aberration corrected HRTEM image of a [1 0 0] fct FePt particle on MgO.

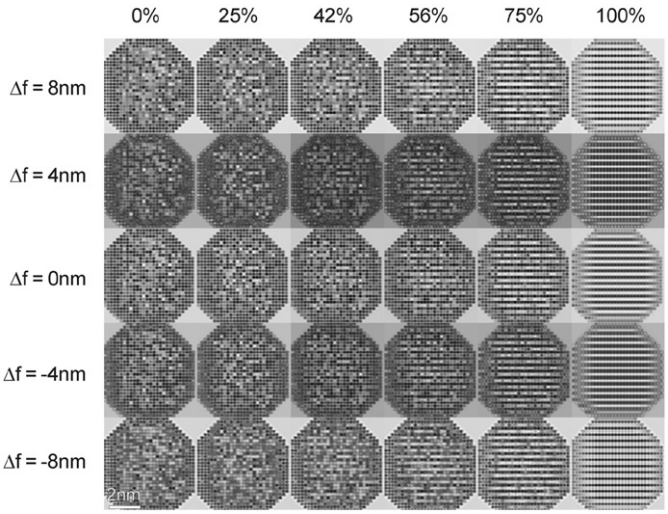

Fig. 2. Focus series of aberration corrected HRTEM image calculations of [1 0 0] FePt nanoparticles with various chemical degree of order (from left to right: 0% corresponds to disordered fcc lattice (Fe and Pt atoms randomly distributed), 100% to perfect ordered fct lattice (one plane Fe atoms, next plane Pt atoms)). Calculation parameters: Doyle–Turner scattering potential, $E=300$ kV, $C_S=-5$ μm.

an inverse FFT has been calculated. The intensity of Fe and Pt columns was determined on the unprocessed STEM images applying the following procedure: via a Gatan Digital Micrograph script based on geometrical phase analysis (GPA) [25] the actual position of the Pt and Fe columns was determined (GPA was basically developed by Hytch to measure strain in HRTEM images [25]; here it is used to determine basically the STEM distortions and find the correct position of the single columns within the images). Then the intensity of each single Fe and Pt column was automatically measured by summing up the Fe and Pt signal within a 3 pixel wide aperture around the columns in real space (3 pixel corresponds to 0.03 nm; a sampling of 0.01 nm/pixel was used during STEM acquisition. The distance between two adjacent Fe and Pt columns is 0.18 nm, respectively, 18 pixel). The average value of intensities between the columns was subtracted as background (I_{bg}) from the column signal. The ratio of intensity was finally calculated by $I_{Fe/Pt}=(I_{Fe}-I_{bg})/(I_{Pt}-I_{bg})$.

The atomic models of FePt particles were prepared using a custom-made program. Image calculations have been carried out using the program MUSLI [26]. The sizes of the matrices for the FFT calculation were chosen to be 512×512 (free standing particles), respectively, 1024×1024 (particles embedded in amorphous SiO_2) resulting in a sampling size of smaller than 0.01 nm/pixel. HRTEM imaging parameters were applied to fit to the experimental data: $C_S=-5$ μm and small steps for defocus (some nanometers). For calculation of Z-contrast STEM images, thermal diffuse scattering using frozen phonon model has been applied [27,28]. The collection angle for scattered electrons was chosen to be the same as in the experiments (40–200 mrad).

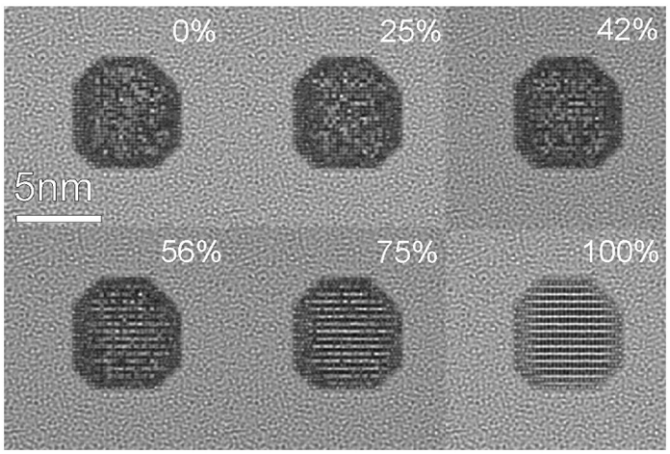

Fig. 3. Aberration corrected HRTEM image calculation of [1 0 0] FePt nanoparticles with various chemical degree of order embedded in amorphous SiO_2. Calculation parameters: Doyle–Turner scattering potential, $E=300$ kV, $C_S=-5$ μm, Focus -4 nm.

3. Results and discussion

Fig. 1a shows an overview bright-field TEM image of FePt particles on (1 0 0) MgO. The particles have an average size of 5 nm in diameter. Fig. 1b shows an aberration corrected HRTEM image of one FePt particle. The particle is aligned along the MgO substrate. The particle shows the typical lattice fringes of the fct-crystal with (0 0 1) planes parallel to the surface, (the substrate–particle orientation relationship is: $(1\,0\,0)_{FePt}//(1\,0\,0)_{MgO}$, $(0\,1\,0)_{FePt}//(0\,1\,0)_{MgO}$ and $(0\,0\,1)_{FePt}//(0\,0\,1)_{MgO}$).

In the next step, HRTEM image calculations have been carried out to analyze whether or not aberration corrected HRTEM lattice fringe contrast allows to determine the degree of chemical order

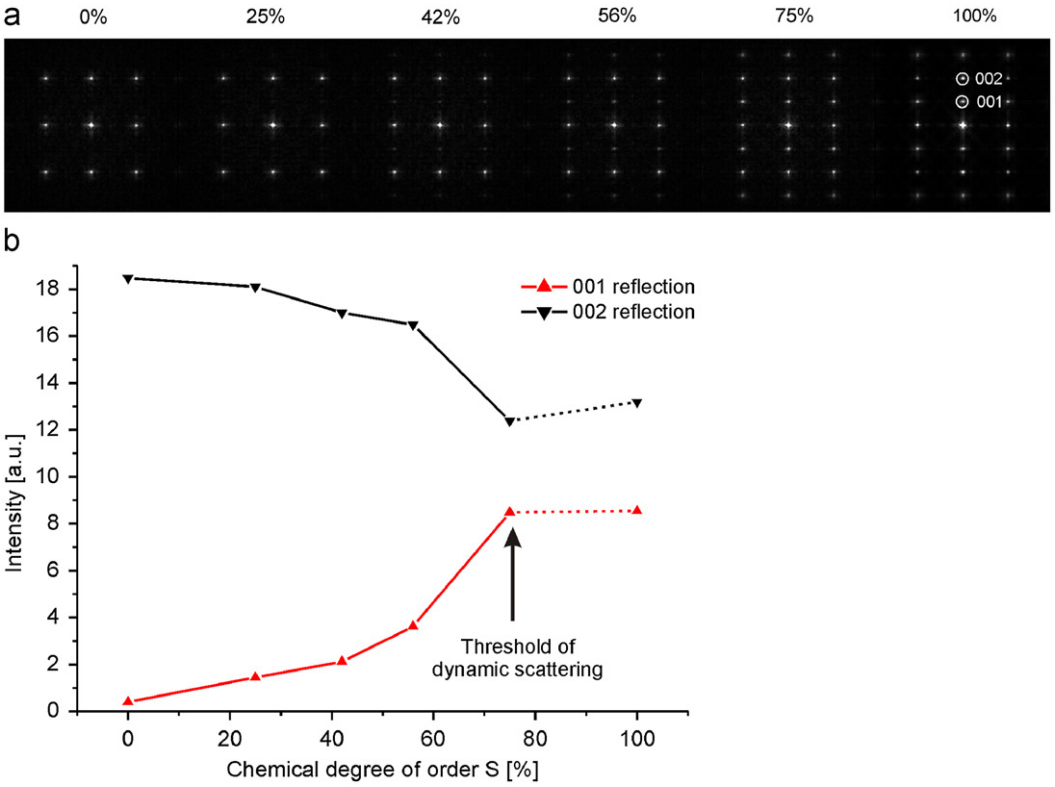

Fig. 4. (a) Calculated electron diffraction patterns of FePt particles containing various degree of chemical degree of order S (left 0% (fcc), right 100% (fct)) and (b) the intensity of (0 0 2) reflection (valid for fcc and fct) and (0 0 1) reflection valid for fct (kinematical diffraction case) is plotted versus the chemical degree of order. Dynamic scattering is dominant above 75%, therefore the curve is marked by the dotted line only.

S. To evaluate the contrast of fct particle-superlattice-reflections in more detail, crystal models of FePt nanoparticles with similar size and shape of the particle shown in Fig. 1b have been calculated. The models contain different degrees of chemical ordering ranging from fcc (0% ordering, left column of particles in Fig. 2) up to fct structure (100% ordering, right column of particles in Fig. 2). Ordering between 0% and 56% predominantly shows the column contrast of the (0 0 2) reflection with varying local changes depending on the focus. The influence of the (0 0 1) reflection can be seen in the HRTEM images at ordering of 75–100%. But only at 100% ordering (pure fct structure) a regular and uniform contrast of the atomic columns is present. For better fitting of the contrast features between experiment and simulations, the thickness of the amorphous background of the SiO_2 protection layer has to be known. Its influence is demonstrated by additional image simulation shown in Fig. 3, where the FePt particle model has been embedded in an amorphous SiO_2 matrix. It is seen that additional blurring of the atomic columns appears and the qualitatively best focus is −4 nm in contrary to the free-standing particle with +4 nm. Because of the irregularities in contrast to the atomic columns, which not only depends on ordering but on focus, thickness and amorphous background, plots of intensities are not reasonable. However, by careful investigation of the contrast details, the experiment shown in Fig. 1b could be fitted to an order parameter *S* of the particle ranging between 56% and 75%.

In addition, more parameters are able to change the HRTEM contrast such as mistilt and strain within the particles because of lattice mismatch between MgO and FePt. Therefore, the use of aberration-corrected HRTEM imaging to determine the degree of chemical order *S* of FePt in exact numbers is not conclusive without further image analysis and extensive image calculations.

Next, it has been evaluated whether or not selected area electron diffraction (SAED) is a possible and an applicable (fast) method to determine quantitatively the order parameter *S*. Fig. 4a shows calculated diffraction patterns of 5 nm FePt particles with different degrees of chemical order. The intensities of (0 0 2) (valid for fcc and fct) and (0 0 1) (valid for fct) reflections are plotted versus *S* in Fig. 4b. At about $S=75\%$ ordering, the slopes of the curves drastically change. This can be interpreted as an effect of dynamic scattering. It is interesting to note that here the dynamic scattering is not thickness dependent (all particles have the same thickness). The dynamic scattering depends on the local (ordering) distribution of strong scattering (Pt) and weak scattering atoms (Fe). This indicates that even for small particles (diameter 5 nm) and high accelerating voltage (300 kV), electron diffraction cannot be applied without considering dynamic scattering to determine the parameter *S* when measuring the ratio between (0 0 1) and (0 0 2) reflections. Taken the dynamic scattering into account, the exact thickness of the particle has to be known and included into a full dynamic calculation such as in the case of HRTEM imaging.

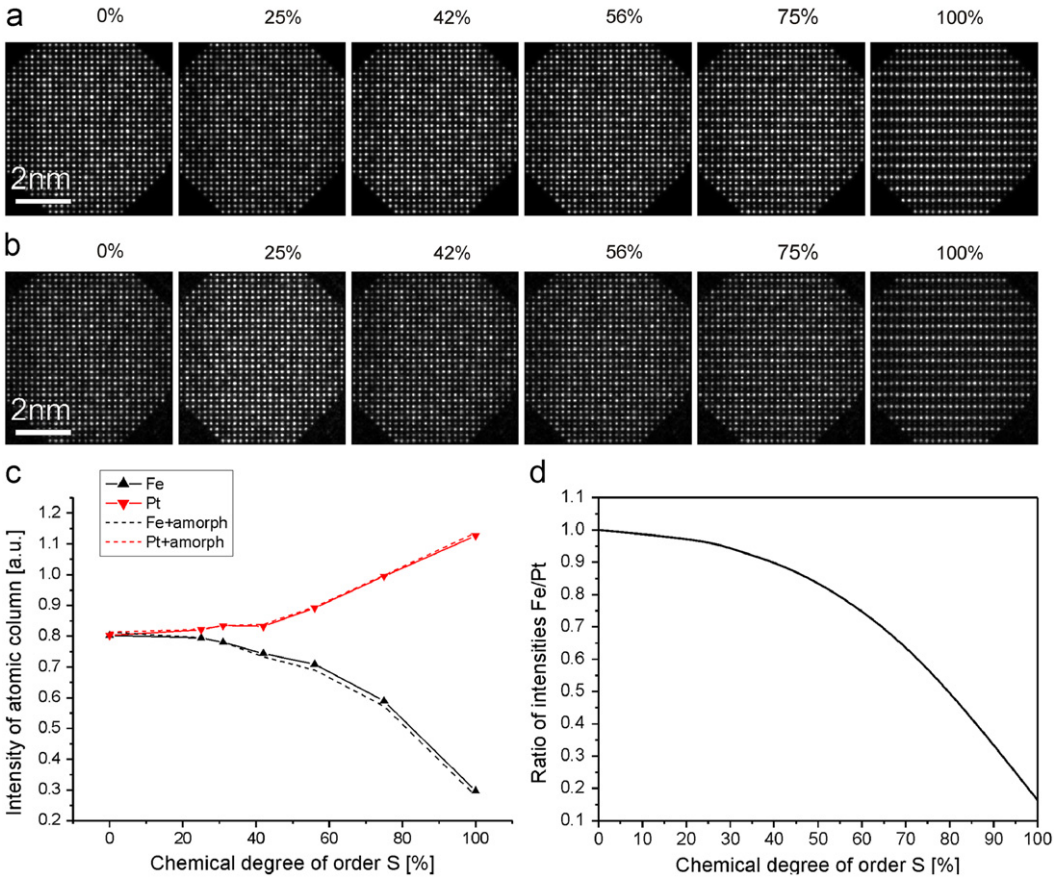

Fig. 5. (a) Calculated HAADF-STEM images of freestanding FePt particles with varying chemical degree of order *S*, (b) calculated HAADF-STEM images of FePt particles with varying chemical degree of order *S* additionally embedded into amorphous SiO_2. The contrast between the columns increases with increase of ordering in both sets of images, (c) plot of the intensities of Fe and Pt column versus the chemical degree of order *S*. At 0% ordering, Pt and Fe column cannot be distinguished. The amorphous SiO_2 has an insignificant effect on the intensity of Fe and Pt columns (dashed curves) and (d) plot of the ratio of intensities of Fe/Pt column versus the order degree using the data of the free standing particles.

Now it will be evaluated whether or not aberration corrected Z-contrast STEM has the sensitivity to correctly determine S in a wide range. Fig. 5a shows calculated Z-contrast STEM images of freestanding FePt nanoparticles. In Fig. 5b the particles are embedded into amorphous SiO_2 (same models were used as shown in Fig. 3). As in the case of HRTEM calculation (compare Figs. 2 and 3), the contrast between the atomic columns increases with increase of S. Already at $S=75\%$ Fe and Pt atom columns can easily be distinguished by naked eye inspection. The contrast between Fe and Pt columns of the embedded nanoparticles (Fig. 5b) seems to be weaker but this is an artefact of the limited colorspace (256 greyscales) and the linear scaling of greyscales. The plots in Fig. 5c show the intensities of the atomic columns as a function of S. The signal of the Pt column steadily increases with S, while the signal of the Fe column lowers accordingly. Here, it can be seen that the underground of amorphous SiO_2 does only insignificantly affect the intensities of Fe and Pt (dashed curves in Fig. 5c). Finally, in Fig. 5d the ratio of intensities of Fe/Pt as a function of S is shown. This graph can be used as a calibration curve to determine S. It should therefore be possible to determine S by simply measuring the ratio of intensity of Fe/Pt columns in STEM image that offers sufficient resolution and signal-to-noise ratio. One may note that the error bar of such type of analysis is rather large for low values of S while for $S>30\%$, a steeper slope is observed resulting in a more precise evaluation of S.

Experiments with aberration corrected STEM on FePt films have been recorded in order to test this method. Prior to the STEM experiments, the FePt film was investigated by X-ray diffraction and S has been determined to be $(65\pm2)\%$. However, the actual accuracy of X-ray diffraction measurements in terms of S determination is limited in case of epitaxially grown thin FePt films on MgO, as described before. An aberration corrected STEM image of a FePt film is shown in Fig. 6a. Even with a corrected STEM system that delivers a nominal point-to-point resolution better than 0.1 nm and high current densities, the signal-to-noise-ratio is still weak. Moreover, the experiment was complicated by drifting first order astigmatism caused probably by the strong magnetic stray field of the sample. However, filtering the image and removing high frequency noise using a Wien-filter, finally allows resolving the weaker Fe columns clearly (see noise filtered image in Fig. 6b). Fig. 6c shows a local map of the intensity ratio between Fe and Pt columns. Each pixel of Fig. 6c stands for a pair of adjacent Fe and Pt columns. For the whole image an average ratio of intensities of Fe/Pt columns was determined to be 0.47 ± 0.05 ($I_{Pt}=1.0$, $I_{Fe}=0.55$, $I_{bg}=0.15$; intensities were normalized to $I_{Pt}=1.0$; all data are averages using root mean square). A local map of the parameter S was calculated using the calibration curve presented in Fig. 5c. The map is shown in Fig. 6d. The average order parameter is $S=(81\pm7)\%$. The ratio of intensities and the parameter S varies over the images. The reason for the variation of intensity ratio and S could be a real variation of the ordering on the nanoscale. Another explanation could be sample bending that results in small mistilts from the [1 0 0] zone axis of FePt that could change contrast of Fe and Pt columns [18].

The average value of $S=(81\pm7)\%$ differs slightly from the results obtained by X-ray diffraction. X-ray diffraction averages on a larger size scale, has limitations if lattice strain is involved, is not applicable on nanoparticles, and cannot detect local changes. Our investigations showed that corrected STEM is a feasible and reasonable approach to measure on the nanoscale level the degree of ordering S.

Our on-going investigations are focused on clarifying how the method can be enhanced in terms of accuracy and reliability.

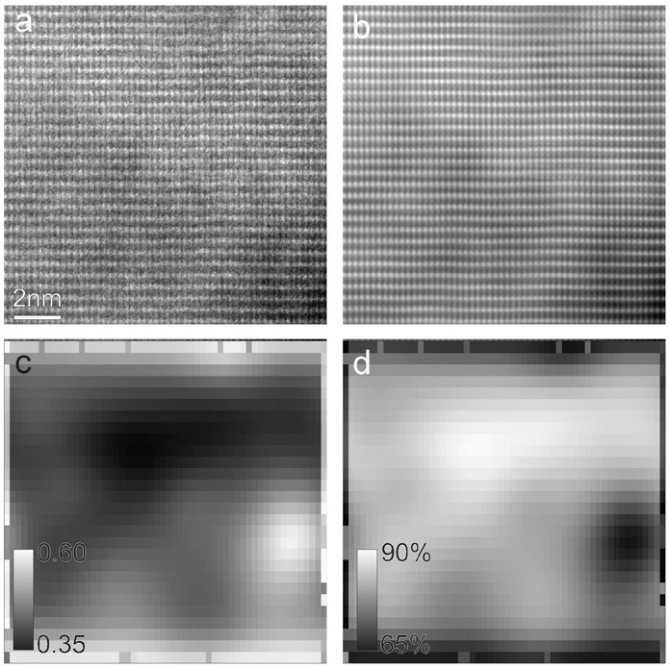

Fig. 6. (a) Aberration corrected STEM image of a FePt film and (b) Wien-filtered image of the original data shown in and (c) map of the intensity ratio of Fe/Pt columns using the data of (a). Each pixel stands for the intensity ratio of a pair of adjacent Fe and Pt columns. The grey values correspond to magnitude of the ratio and are indicated by the scalebar and (d) map of the chemical degree of order S, the marked areas of the STEM image. The grey values that correspond to the magnitude of S are indicated by the scalebar. S was determined to be 81% for the whole image. Please note that the border pixel of (c,d) contains artefacts.

4. Summary

In FePt nanoparticles and films, the structural property chemical degree of order (S) is linked to the magnetic behaviour. $S=0\%$ is linked to fcc phase with a low magnetocrystalline anisotropy energy density (MAE), $S=100\%$ to the perfect fct phase with a very high MAE.

We evaluated aberration corrected HRTEM, electron diffraction and aberration corrected HAADF-STEM as methods to measure the chemical degree of order S, and thereby the magnetic property of FePt nanoparticles and thin films. HRTEM and electron diffraction suffer from dynamic scattering and are not suitable fast methods unless other parameters such as diameter or thickness of the particles are exactly determined and full dynamic calculations have been carried out. Z-contrast STEM is more rigid against dynamic scattering, scales linearly with thickness and is the method of choice to determine S. Using a curve based on image calculation as calibration standard, the parameter S could be locally determined on a nanoscale.

Acknowledgements

We acknowledge the financial support of the Deutsche Forschungsgemeinschaft DFG within the collaborative research network SFB 569. We thank S. Grözinger (Ulm University) for supporting TEM sample preparation. We are grateful to Prof. R. Dunin-Borkowski (Center for Electron Nanoscopy (Cen) at Denmark Technical University) for allowing using the microscopes at DTU. We are grateful to Dr. A. Chuvilin (CIC nanoGUNE, San Sebastian) for supporting DM3 scripting.

References

[1] S. Sun, Recent advances in chemical synthesis, self-assembly, and applications of FePt nanoparticles, Advanced Materials 18 (2006) 393–403 and references within.

[2] S.D. Bader, Opportunities in nanomagnetism, Reviews of Modern Physics 78 (2006) 1–15 and references within.

[3] G. Reiss, A. Hütten, Magnetic nanoparticles: applications beyond data storage, Nature Materials 4 (2005) 725–726.

[4] A. Ethirajan, U. Wiedwald, H.-G. Boyen, B. Kern, L. Han, A. Klimmer, F. Weigl, G. Kästle, P. Ziemann, K. Fauth, C. Jun, J. Behm, P. Oelhafen, P. Walther J. Biskupek, U. Kaiser, A micellar approach to magnetic ultra-high density data storage media—extending the limits of current colloidal methods, Advanced Materials 19 (2007) 406–417.

[5] A. Terheiden, C. Mayer, K. Moh, B. Stahlmecke, S. Stappert, M. Acet B. Rellinghaus, Postdeposition organic coating and self-assembly of gas phase prepared FePt nanoparticles on lipid reservoir films, Applied Physics Letters 84 (2004) 3891–3894.

[6] K. Watanabe, H. Masumoto, On the high-energy product Fe–Pt permanent magnet alloys, Transactions of the Japan Institute of Metals 9 (1983) 627–632.

[7] C.-B. Rong, Y. Li, J.P. Liu, Curie temperatures of annealed FePt nanoparticle systems, Journal of Applied Physics 101 (2007) 09K505.

[8] L. Han, U. Wiedwald, B. Kuerbanjiang, P. Ziemann, Fe oxidation versus Pt segregation in FePt nanoparticles and thin films, Nanotechnology 20 (2009) 285706.

[9] U. Wiedwald, A. Klimmer, B. Kern, L. Han, H.-G. Boyen, P. Ziemann, K. Fauth, Lowering of the L10 ordering temperature of FePt nanoparticles by He+ ion irradiation, Applied Physics Letters 90 (2007) 062508.

[10] A. Menshikov, T. Tarnoczi, E. Kren, Magnetic structure of ordered Fe Pt and Fe3 Pt alloy, Physica Status Solidi, Sectio A: Applied Research 28 (1975) 85–87.

[11] G.P. Gasnikova, Y.A. Dorofeev, A.Z. Men'shikov, S.K. Sidorov, Magnetic phase transitions in ordered (Fe1−*x* Mn*x*) Pt alloys, Physics of Metals and Metallography 55 (1983) 86–91.

[12] R.E. Dunin-Borkowski, T. Kasama, R.J. Harrison, in: A.I. Kirkland, J.L. Hutchison (Eds.), Electron Holography of Nanostructured Materials in Nanocharacterisation, Royal society of chemistry, 2007, pp. 138–183.

[13] J. Biskupek, U. Kaiser, H. Lichte, A. Lenk, T. Gemming, T.G. Pasold W. Witthuhn, TEM-characterization of magnetic samarium- and cobalt-rich-nanocrystals formed in hexagonal SiC, Journal of Magnetism and Magnetic Materials 293/3 (2005) 924–937.

[14] M. Haider, H. Rose, S. Uhlemann, E. Schwan, B. Kabius, K. Urban, A spherical-aberration-corrected 200 kV transmission electron microscope, Ultramicroscopy 75 (1998) 53–60.

[15] N. Delby, O.I. Krivanek, P.D. Nellist, P.E. Batson, A.R. Lupin, Progress in aberration corrected scanning transmission electron microscopy, Journal of Electron Microscopy 50 (2001) 177–185.

[16] M. Lentzen, B. Jahnen, C.L. Jia, A. Thus, K. Tillmann, K. Urban, High resolution imaging with an aberration-corrected transmission electron microscope, Ultramicroscopy 92 (2002) 233–242.

[17] O. Dmitrieva, M. Acet, G. Dumpich, J. Kästner, C. Atoniak, M. Farle, K. Fauth, Enhancement of L10 phase formation in FePt nanoparticles by nitrogenization, Journal of Physics D: Applied Physics 39 (2006) 4741–4745.

[18] O. Dmitrieva, B. Rellinghaus, J. Kästner, M.O. Liedke, J. Fassbender, Ion beam induced destabilization of icosahedral structures in gas phase prepared FePt nanoparticles, Journal of Applied Physics 97 (2005) 10N112.

[19] O. Dmitrieva, B. Rellinghaus, J. Kästner, G. Dumpich, Quantitative structure analysis of L10-ordered FePt nanoparticles by HRTEM, Journal of Crystal Growth 303 (2007) 645–650.

[20] A. Kovacs, K. Sato, V.K. Lazarov, P.L. Galindo, T.J. Konno, Y. Hirotsu, Direct observation of a surface induced disordering process in magnetic nanoparticles, Physical Review Letters 103 (2009) 115703.

[21] K. Sato, J.G. Wen, J.M. Zuo, Intermetallic ordering and structure in FePd alloy nanoparticles, Journal of Applied Physics, 105 (200), 093509.

[22] K. Sato, T.J. Konno, Y. Hirotsu, Atomic structure imaging of L10-type FePd nanoparticles by spherical aberration corrected high-resolution transmission electronmicroscopy, Journal of Applied Physics 105 (2009) 034308.

[23] M. Bendele, Optimierung eptiaktischer FePt-Filme, Diploma thesis, Ulm University, D-89069 Ulm, Germany 2009.

[24] M. Lentzen, The tuning of a Zernike phase plate with defocus and variable spherical aberration and its use in HRTEM imaging, Ultramicroscopy 99 (2004) 211–220.

[25] M.J. Hytch, Analysis of variations in structure from high resolution electron microscope images by combining real space and Fourier space information, Microscopy Microanalysis Microstructures 8 (1997) 41–57.

[26] U. Kaiser, A. Chuvilin, On the peculiarities of CBED pattern formation revealed by multislice simulation, Ultramicroscopy 104 (2005) 73–82.

[27] J. Biskupek, A. Chuvilin, U. Kaiser, Evaluation of frozen phonon models for multislice calculation of TDS, Microscopy and Microanalysis 13 (2007) 130–131.

[28] L.J. Allen, S.D. Findlay, M.P. Oxley, C.J. Rossouw, Lattice-resolution contrast from a focused coherent electron probe, Part I & II, Ultramicrosopy 96 (2003) 47–81.